

Development and Assessment of Simplified Models for Dynamic Analyses of Bridge Piers Subjected to Barge Impact

DISSERTATION

zur Erlangung des akademischen Grades
Doktor-Ingenieur (Dr.-Ing.)

an der Fakultät Bauingenieurwesen
der Bauhaus-Universität Weimar

vorgelegt von

Wei Wang

geboren am 20. Oktober 1989
in An Hui Province, China

Mentor: Prof. Dr. Guido Morgenthal

Weimar, August 2018

Declaration

I hereby declare that I have made this work without undue assistance from third parties and without the use of other than the referenced sources. The data and concepts taken directly or indirectly from other sources are indicated using corresponding references.

Other people were not involved in the development of the content of this work. I have not used any paid help for mediation or consultancy services (promotion consultants or other persons). No one has ever received direct or indirect financial benefit related to the content of this submitted dissertation. This work has not been previously submitted anywhere else for any purpose.

I confirm on my honor that what has been said is true and nothing has been concealed.

Place, Date

Signature

Ehrenwörtliche Erklärung

Ich erkläre hiermit ehrenwörtlich, dass ich die vorliegende Arbeit ohne unzulässige Hilfe Dritter und ohne Benutzung anderer als der angegebenen Hilfsmittel angefertigt habe. Die aus anderen Quellen direkt oder indirekt übernommenen Daten und Konzepte sind unter Angaben der Quellen gekennzeichnet.

Weitere Personen waren an der inhaltlich-materiellen Erstellung der vorliegenden Arbeit nicht beteiligt. Insbesondere habe ich hierfür nicht die entgeltliche Hilfe von Vermittlungs- bzw. Beratungsdiensten (Promotionsberater oder anderer Personen) in Anspruch genommen. Niemand hat von mir unmittelbar oder mittelbar geldwerte Leistungen für Arbeiten erhalten, die im Zusammenhang mit dem Inhalt der vorgelegten Dissertation stehen. Die Arbeit wurde bisher weder im Innoch im Ausland in gleicher oder ähnlicher Form einer anderen Prüfungsbehörde vorgelegt.

Ich versichere ehrenwörtlich, dass ich nach bestem Wissen die reine Wahrheit gesagt und nichts verschwiegen habe.

Ort, Datum

Unterschrift

Acknowledgements

First and foremost I would like to express my deep gratitude to my supervisor Prof. Dr. Guido Morgenthal for his sustained guidance, his support and his inspiration throughout my four-year PhD studies. His great patience and understanding enabled me to achieve continuous progress in my research.

I am sincerely thankful for Prof. Dr. Junjie Wang and Prof. Dr. Matthias Kraus for taking the time to review my work. I would like to express my deep gratitude to my colleagues. Their enthusiasm, hospitality and frankness made my life enjoyable, interesting and passionate. Their endless help and sharing greatly enriched my life. Particular thanks must go to Dr. Hans-Georg Timmler for his helpful comments regarding my work and dissertation.

I would like to thank my friend Yanchen Song from Tongji University for helping me with the software. I would like to thank my friend Yanyan Sha from Norwegian University of Science and Technology for sharing his experience in my research topic. I would also like to thank my senior colleague Tajammal Abbas for helping me with the dissertation.

I am sincerely thankful for the China Scholarship Council for providing the financial support for my studies.

Last but not least, I owe a lot of debts to my parents who are always there for me. Their endless care, love and encouragement are great motivations for me in life. I am also grateful to my girlfriend Yuehong Lu who is always positive and passionate. Her unconditional understanding and encouragement imbued me with passion and energy to pursue our dreams and ideals together.

Wei Wang
Weimar, 2018

Abstract

Barge impact is a potential hazard for bridge piers located in navigation waterways. The prediction of impact force and dynamic pier responses is important for bridge designs against barge impact. The main objective of the dissertation is to develop simplified models to efficiently predict the dynamic impact process with sufficient accuracy and to use such simplified models to devise crashworthy devices for pier protection and conduct reliability analyses of bridge piers subjected to barge impact.

In this study, the complex finite-element (FE) barge model is developed with calibrations against one literature barge model. The full barge impact model (FBIM) using the proposed barge model and rigid pier column is developed to study the influences of pier shape, pier size, impact velocity and impact angle upon the barge crushing behavior.

As FE simulation requires high computational cost, a simplified mass-spring model (MSM) is developed to replicate the complex barge model. The MSM models the barge mass using a lumped mass and the barge bow plasticity using non-linear springs. By coupling MSM with rigid pier column, a simplified impact model (SIM) is developed to generate the MSM parameters by the optimization model which aims to minimize the integration error of impact force time-histories predicted by FBIM and SIM, respectively.

In order to efficiently predict the dynamic impact process with sufficient accuracy, the coupled multi-degree-of-freedom model (CMM) is developed by coupling MSM with the pier column at the impact position. The CMM models the pier column using discrete masses and beam elements. The prediction quality of CMM is thoroughly assessed for a wide range of impact scenarios using linear elastic pier columns.

Material non-linearity of pier column members, which is influential upon the dynamic impact process, is considered by CMM using fibre beam elements. The numerical RC pier column model, which is developed based on the numerical RC beam model validated by experimental impact tests, is used in FBIM. The FBIM is then used as the benchmark model to assess the prediction quality of CMM for a wide range of impact scenarios involving material non-linearity of pier column members.

Using the proposed simplified models, parametric studies are conducted to evaluate the energy-dissipation capacity of pile-supported independent protective structures which are widely used in bridge designs against barge impact. In addition, a new type of crashworthy device comprised of a supported or floated cap connected to the bridge pier using a series of steel beams of I-cross-section is devised and its effectiveness is investigated using the proposed simplified models. To achieve cost-optimum design of the proposed crashworthy device for a given impact scenario, an optimization model is developed with constraints generated by the prescribed design requirements.

Due to the non-deterministic nature of barge impact scenario and pier resistance, reliability analyses of RC pier column subjected to barge impact are conducted using the proposed simplified models with existing reliability methods and sensitivity analyses are conducted to figure out the sensitive random variables.

Keywords: Full barge impact model, Mass-spring model, Simplified impact model, Coupled multi-degree-of-freedom model, Crashworthy device, Reliability analyses.

Contents

Abstract	viii
List of Figures	xii
List of Tables	xx
List of Symbols	xxi
List of Acronyms	xxiv
1 Introduction	1
1.1 Motivation for Research	1
1.2 Objective of Research	3
1.3 Contribution of Research	3
1.4 Organization of Dissertation	4
2 Literature Review	6
2.1 Introduction	6
2.2 Strategies for Vessel Impact Analyses	6
2.2.1 Experimental Impact Tests	6
2.2.2 Empirical Formulas	9
2.2.2.1 The AASHTO Guide Specification	9
2.2.2.2 The Eurocode	10
2.2.3 Finite-Element Simulations	11
2.2.4 Simplified Impact Models	12
2.3 Protective Structures for Vessel Impact	14
2.4 Reliability Analyses of Bridge Pier Subjected to Vessel Impact	16
3 Complex Full Barge Impact Model	17
3.1 Introduction	17
3.2 Barge Configurations	17
3.3 Material Models	18
3.4 Contact Definition and Mesh Sizes	20
3.5 Calibration of Complex Barge Model	20
3.6 Simulations of Head-on Impact Scenarios	21
3.7 Simulations of Oblique Impact Scenarios	28
3.8 Summary	30
4 Simplified Mass-Spring Model Coupled with Rigid Pier Column	32
4.1 Introduction	32
4.2 Basic Descriptions of MSM	32
4.3 Equations of Motion	34
4.4 Determination of MSM Parameters	34
4.4.1 Benchmark Simulations	34

4.4.2	Strategies for Determining MSM Parameters	34
4.5	Regression Formulas for Calculating MSM Parameters	37
4.5.1	Head-on Impact Scenarios	37
4.5.2	Oblique Impact Scenarios	40
4.6	Summary	42
5	Coupled Multi-Degree-of-Freedom Model Using Linear Elastic Pier Column	43
5.1	Introduction	43
5.2	Equations of Motion	43
5.3	Assessment of CMM Prediction Quality	45
5.3.1	Head-on Impact Scenarios	45
5.3.2	Oblique Impact Scenarios	65
5.4	Parametric Studies	75
5.4.1	Barge Mass	75
5.4.2	Impact Velocity	75
5.4.3	Impact Position	77
5.4.4	Pier Stiffness	78
5.5	Summary	81
6	Material Non-Linearity of Pier Column Members	82
6.1	Introduction	82
6.2	Calibration of Concrete Model	82
6.3	Development of RC Pier Column	86
6.4	CMM Using Fibre Beam Elements	87
6.4.1	Model Assumptions	87
6.4.2	Equations of Motion	88
6.4.3	State Determination of Beam Element	88
6.4.4	Stress-Strain Relationships of Concrete and Reinforcement Steel	90
6.5	Parametric Studies	91
6.5.1	Barge Mass	93
6.5.2	Impact Velocity	93
6.5.3	Impact Position	93
6.5.4	Pier Height	95
6.5.5	Longitudinal Reinforcement Diameter	97
6.6	Consideration of Pier Shape and Pier Size	102
6.6.1	Configuration of RC Pier Columns	102
6.6.2	Simulated Impact Scenarios	103
6.6.3	Simulation Results	105
6.7	Summary	108
7	Evaluation of Pile-Supported Independent Protective Structures Using Simplified Models	109
7.1	Introduction	109
7.2	Configuration of Structure	109
7.3	Simplified Impact Model	109
7.4	Non-Linear Soil Spring Models	110
7.4.1	Force-Deformation Relationships of Non-Linear Soil Springs	110
7.4.2	Unloading Properties of Non-Linear Soil Springs	113
7.5	Stress-Strain Relationships of Pipe-Confined Concrete and Pipe Steel	113

7.6	Parametric Studies	114
7.6.1	Diameter of Pile Cross-Section	115
7.6.2	Pile Length	115
7.6.3	Pipe Thickness	116
7.6.4	Scour Depth	117
7.6.5	Impact Velocity	117
7.7	Summary	122
8	Development and Evaluation of New Crashworthy Device Using Simplified Models	123
8.1	Introduction	123
8.2	Configuration of Structure	123
8.3	Simplified Impact Model	124
8.4	Parametric Studies	125
8.4.1	Beam Cross-Section Dimension	126
8.4.2	Yielding Strength of Beam Steel	127
8.4.3	Number of Beam Units	130
8.4.4	Impact Velocity	133
8.5	Optimum Configuration of Cap-Steel-Beam Structure	140
8.5.1	Mathematical Optimization Model	140
8.5.2	Application Example	141
8.6	Discussion	146
8.7	Summary	147
9	Reliability Analyses of RC Pier Column Subjected to Barge Impact	148
9.1	Introduction	148
9.2	The RC Pier Column Model	148
9.3	Simplified Impact Model	149
9.4	Pile-Group Effects	150
9.5	Methods for Reliability Analyses	151
9.5.1	Standard Monte Carlo Method	151
9.5.2	Response Surface Method	151
9.6	Randomness of Variables	152
9.7	Limit State Functions	153
9.8	Results and Discussions	153
9.8.1	Reliability Indexes	153
9.8.2	Sensitivity Analyses	154
9.9	Summary	155
10	Conclusions and Outlook	156
10.1	Summary	156
10.2	Conclusions	157
10.3	Recommendations for Further Research	159
	Bibliography	160
	Publications by the Author	168

List of Figures

1.1	Collapse of Queen Isabella Causeway after being hit by four loaded barges on 15 September 2001	1
1.2	Collapse of I-40 highway bridge after being hit by two barges on 26 May 2002	2
1.3	Collapse of Jiujiang Bridge after being hit by the cargo vessel on 15 June 2007	2
2.1	Strategies for vessel-pier impact analyses	6
2.2	Relationship of hammer impact energy, barge bow crushing depth and impact force based on the impact tests conducted by Meir-Dornberg . . .	7
2.3	Bridge piers selected for conducting the barge impact tests	8
2.4	Barge impact tests on Pier-1 and Pier-3 of the old St. George Island Causeway Bridge	8
2.5	Impact force time-history determined by Eurocode for vessels traveling in inland waterways	11
2.6	Coupling between the barge and the pier using the CVIA technique . . .	13
2.7	Yuan’s simplified model using elastoplastic-collapse elements	13
3.1	Configuration of Jumbo Hopper barge	17
3.2	The complex finite-element barge model	18
3.3	Stress-strain relationship of barge steel	19
3.4	Full barge impact models using rigid flat pier column and rigid circular pier column, respectively	19
3.5	Crushing of barge bow after impact	21
3.6	Time-histories of impact force and barge bow crushing depth corresponding to rigid flat pier columns for head-on impact using fully loaded barge . .	23
3.7	Time-histories of impact force and barge bow crushing depth corresponding to rigid circular pier columns for head-on impact using fully loaded barge	24
3.8	Maximum impact force and maximum barge bow crushing depth vs. impact velocity corresponding to rigid flat pier columns for head-on impact using fully loaded barge	25
3.9	Maximum impact force and maximum barge bow crushing depth vs. impact velocity corresponding to rigid circular pier columns for head-on impact using fully loaded barge	25
3.10	Barge bow force-deformation relationships for the whole impact process and for the first 0.10 m of barge bow deformation corresponding to rigid flat pier columns for head-on impact using fully loaded barge	26
3.11	Barge bow force-deformation relationships for the whole impact process and for the first 0.10 m of barge bow deformation corresponding to rigid circular pier columns for head-on impact using fully loaded barge	27
3.12	Simulation of oblique impact scenario using full barge impact model . . .	28
3.13	Maximum impact force vs. impact angle corresponding to different impact velocities using fully loaded barge and pier column $RP_F^{0.3}$	29

3.14	Barge bow force-deformation relationships corresponding to different impact angles using fully loaded barge and pier column $RP_F^{0.3}$	30
4.1	General shape of barge bow force-deformation curve	33
4.2	Simplified mass-spring model coupled with rigid pier	33
4.3	Bi-linear spring model and triangular spring model	33
4.4	The loading, unloading and reloading processes of first non-linear spring .	34
4.5	Impact force time-histories, barge bow crushing depth time-histories and barge bow force-deformation curves corresponding to different impact velocities for head-on impact using fully loaded barge and rigid flat pier column	35
4.6	Barge bow force-deformation curves within 0.10 m of barge bow deformation corresponding to different impact velocities for head-on impact using fully loaded barge and rigid flat pier column	36
4.7	MSM parameter F_{sp} vs. prescribed constant velocity v_p and the regression curves using different fitting functions for head-on impact using fully loaded barge and rigid flat pier column	37
4.8	MSM parameters F_{sy} and F_{su} vs. pier width/diameter to barge width ratio corresponding to two pier column shapes for head on impact	38
4.9	MSM parameter F_{sp} vs. prescribed constant velocity v_p corresponding to rigid flat pier columns and rigid circular pier columns, respectively, for head-on impact using fully-loaded barge	39
4.10	MSM parameter F_{sp} vs. prescribed constant velocity v_p corresponding to different pier width to barge width ratios and impact angles using fully loaded barge	41
5.1	Transformation of FBIM into CMM	44
5.2	Time-histories of column top displacement determined by FBIM and by imposing the impact force time-history generated by FBIM on the impact position of the discrete pier column model used in CMM, respectively, using pier column $EP_S^{0.2}$	46
5.3	The integration error of impact force time-history, relative error of maximum impact force and relative error of maximum column top displacement predicted by CMM corresponding to pier column $EP_S^{0.2}$ for different combinations of barge mass and impact velocity	47
5.4	The integration error of impact force time-history, relative error of maximum impact force and relative error of maximum column top displacement predicted by CMM corresponding to pier column $EP_S^{0.3}$ for different combinations of barge mass and impact velocity	48
5.5	The integration error of impact force time-history, relative error of maximum impact force and relative error of maximum column top displacement predicted by CMM corresponding to pier column $EP_S^{0.4}$ for different combinations of barge mass and impact velocity	49
5.6	Impact force time-histories corresponding to pier column $EP_S^{0.2}$ for different combinations of barge mass and impact velocity (head-on impact)	50
5.7	Impact force time-histories corresponding to pier column $EP_S^{0.3}$ for different combinations of barge mass and impact velocity (head-on impact)	51
5.8	Impact force time-histories corresponding to pier column $EP_S^{0.4}$ for different combinations of barge mass and impact velocity (head-on impact)	52

5.9	Time-histories of column top displacement corresponding to pier column $EP_S^{0.2}$ for different combinations of barge mass and impact velocity (head-on impact)	53
5.10	Time-histories of column top displacement corresponding to pier column $EP_S^{0.3}$ for different combinations of barge mass and impact velocity (head-on impact)	54
5.11	Time-histories of column top displacement corresponding to pier column $EP_S^{0.4}$ for different combinations of barge mass and impact velocity (head-on impact)	55
5.12	The integration error of impact force time-history, relative error of maximum impact force and relative error of maximum column top displacement predicted by CMM corresponding to pier column $EP_C^{0.2}$ for different combinations of barge mass and impact velocity	56
5.13	The integration error of impact force time-history, relative error of maximum impact force and relative error of maximum column top displacement predicted by CMM corresponding to pier column $EP_C^{0.3}$ for different combinations of barge mass and impact velocity	57
5.14	The integration error of impact force time-history, relative error of maximum impact force and relative error of maximum column top displacement predicted by CMM corresponding to pier column $EP_C^{0.4}$ for different combinations of barge mass and impact velocity	58
5.15	Impact force time-histories corresponding to pier column $EP_C^{0.2}$ for different combinations of barge mass and impact velocity (head-on impact)	59
5.16	Impact force time-histories corresponding to pier column $EP_C^{0.3}$ for different combinations of barge mass and impact velocity (head-on impact)	60
5.17	Impact force time-histories corresponding to pier column $EP_C^{0.4}$ for different combinations of barge mass and impact velocity (head-on impact)	61
5.18	Time-histories of column top displacement corresponding to pier column $EP_C^{0.2}$ for different combinations of barge mass and impact velocity (head-on impact)	62
5.19	Time-histories of column top displacement corresponding to pier column $EP_C^{0.3}$ for different combinations of barge mass and impact velocity (head-on impact)	63
5.20	Time-histories of column top displacement corresponding to pier column $EP_C^{0.4}$ for different combinations of barge mass and impact velocity (head-on impact)	64
5.21	The integration error of impact force time-history, relative error of maximum impact force and relative error of maximum column top displacement predicted by CMM corresponding to pier column $EP_S^{0.2}$ for different combinations of impact velocity and impact angle using fully loaded barge	66
5.22	The integration error of impact force time-history, relative error of maximum impact force and relative error of maximum column top displacement predicted by CMM corresponding to pier column $EP_S^{0.3}$ for different combinations of impact velocity and impact angle using fully loaded barge	67

5.23	The integration error of impact force time-history, relative error of maximum impact force and relative error of maximum column top displacement predicted by CMM corresponding to pier column $EP_S^{0.4}$ for different combinations of impact velocity and impact angle using fully loaded barge	68
5.24	Impact force time-histories corresponding to pier column $EP_S^{0.2}$ for different combinations of impact velocity and impact angle using fully loaded barge	69
5.25	Impact force time-histories corresponding to pier column $EP_S^{0.3}$ for different combinations of impact velocity and impact angle using fully loaded barge	70
5.26	Impact force time-histories corresponding to pier column $EP_S^{0.4}$ for different combinations of impact velocity and impact angle using fully loaded barge	71
5.27	Time-histories of column top displacement corresponding to pier column $EP_S^{0.2}$ for different combinations of impact velocity and impact angle using fully loaded barge	72
5.28	Time-histories of column top displacement corresponding to pier column $EP_S^{0.3}$ for different combinations of impact velocity and impact angle using fully loaded barge	73
5.29	Time-histories of column top displacement corresponding to pier column $EP_S^{0.4}$ for different combinations of impact velocity and impact angle using fully loaded barge	74
5.30	Time-histories of impact force and column top displacement corresponding to different barge masses	76
5.31	Maximum impact force and maximum column top displacement vs. barge mass	76
5.32	Time-histories of impact force and column top displacement corresponding to different impact velocities	77
5.33	Maximum impact force and maximum column top displacement vs. impact velocity	78
5.34	Time-histories of impact force and column top displacement corresponding to different impact positions	79
5.35	Maximum impact force and maximum column top displacement vs. height of impact position	80
5.36	Time-histories of impact force and column top displacement corresponding to different pier column stiffness	80
5.37	Maximum impact force and maximum column top displacement vs. pier column stiffness	81
6.1	Setup of the drop hammer impact test	83
6.2	High-resolution FE model of the drop hammer impact test	83
6.3	Damage distributions of the RC beams from drop hammer impact tests and from numerical simulations, respectively	84
6.4	Time-histories of impact force and mid-span displacement corresponding to different drop heights	85
6.5	Layout of reinforcement rebars and high-resolution RC pier column model	86
6.6	Nodal DOFs and nodal forces of the beam element with rigid body mode and without rigid body mode, respectively	87
6.7	Stress-strain relationship and unloading properties of concrete	91
6.8	Bi-linear stress-strain relationship of reinforcement steel	91

6.9	Maximum impact forces predicted by FBIM and CMM, respectively, and the ratios of F_{sp} predicted by FBIM to F_{sp} predicted by CMM corresponding to different impact velocities using fully loaded barge	92
6.10	Time-histories of impact force, column top displacement and bending moment at column bottom section corresponding to different barge masses	94
6.11	Maximum impact force, maximum column top displacement and maximum bending moment at column bottom section vs. barge mass	95
6.12	Time-histories of impact force, column top displacement and bending moment at column bottom section corresponding to different impact velocities	96
6.13	Maximum impact force, maximum column top displacement and maximum bending moment at column bottom section vs. impact velocity	97
6.14	Time-histories of impact force, column top displacement and bending moment at column bottom section corresponding to different impact positions	98
6.15	Maximum impact force, maximum column top displacement and maximum bending moment at column bottom section vs. height of impact position	99
6.16	Time-histories of impact force, column top displacement and bending moment at column bottom section corresponding to different pier column heights	100
6.17	Maximum impact force, maximum column top displacement and maximum bending moment at column bottom section vs. pier column height	101
6.18	Time-histories of impact force, column top displacement and bending moment at column bottom section corresponding to different reinforcement rebar diameters	101
6.19	Maximum impact force, maximum column top displacement and maximum bending moment at column bottom section vs. reinforcement rebar diameter	102
6.20	FBIM using RC pier column $RCP_F^{3,0}$ and layout of longitudinal reinforcements	104
6.21	FBIM using RC pier column $RCP_F^{3,0}$ and layout of longitudinal reinforcements	104
6.22	Maximum impact force, maximum column top displacement and maximum bending moment at column bottom section vs. pier width	105
6.23	Maximum impact force, maximum column top displacement and maximum bending moment at column bottom section vs. pier diameter	105
6.24	Time-histories of impact force, column top displacement and bending moment at column bottom section corresponding to different flat RC pier columns	106
6.25	Time-histories of impact force, column top displacement and bending moment at column bottom section corresponding to different circular RC pier columns	107
7.1	Configuration of pile-supported protective structure and pile cross-section	110
7.2	Simplified impact model for pile-supported independent protective structure subjected to barge impact considering soil-pile interactions . . .	111
7.3	Pile tip load-displacement (Q-z) curve and axial pile load-displacement (t-z) curve for sand soil	112
7.4	Loading and unloading property of compression-only soil springs (Q-z springs and p-y springs)	113

LIST OF FIGURES

7.5	Time-histories of cap displacement, energy absorbed by barge bow, energy absorbed by pile and energy absorbed by soil, respectively, corresponding to different pile cross-section diameters	116
7.6	Maximum cap displacement and the energy absorbed by barge bow, by pile and by soil after impact, respectively, vs. pile cross-section diameter	117
7.7	Time-histories of cap displacement, energy absorbed by barge bow, energy absorbed by pile and energy absorbed by soil, respectively, corresponding to different pile lengths	118
7.8	Maximum cap displacement and the energy absorbed by barge bow, by pile and by soil after impact, respectively, vs. pile length	118
7.9	Time-histories of cap displacement, energy absorbed by barge bow, energy absorbed by pile and energy absorbed by soil, respectively, corresponding to different pipe thicknesses	119
7.10	Maximum cap displacement and the energy absorbed by barge bow, by pile and by soil after impact, respectively, vs. pipe thickness	119
7.11	Time-histories of cap displacement, energy absorbed by barge bow, energy absorbed by pile and energy absorbed by soil, respectively, corresponding to different scour depths	120
7.12	Maximum cap displacement and the energy absorbed by barge bow, by pile and by soil after impact, respectively, vs. scour depth	120
7.13	Time-histories of cap displacement, energy absorbed by barge bow, energy absorbed by pile and energy absorbed by soil, respectively, corresponding to different impact velocities	121
7.14	Maximum cap displacement and the energy absorbed by barge bow, by pile and by soil after impact, respectively, vs. impact velocity	122
8.1	The structure connecting the cap and the bridge pier using steel beams of I-cross-section for the bridge pier of Rosario-Victoria Bridge, Argentina	124
8.2	Configuration of cap-steel-beam structure and I-cross-section of steel beams	125
8.3	Simplified impact model for cap-steel-beam structure subjected to barge impact	125
8.4	Energy absorbed by cap-steel-beam structure during impact corresponding to different beam cross-section dimensions	126
8.5	Time-histories of cap displacement corresponding to different beam cross-section dimensions and maximum cap displacement vs. beam cross-section dimension	127
8.6	Maximum bending moment diagrams of the structures during impact and deflections of the structures after impact corresponding to different beam cross-section dimensions	128
8.7	Moment-curvature relationships of the I-cross-sections and moment-rotation relationships of single steel beams corresponding to different beam cross-section dimensions	129
8.8	Impact force time-histories on the bridge pier for the whole impact process, for the first 0.10 s of impact process corresponding to different beam cross-section dimensions and the maximum impact force vs. beam cross-section dimension	129
8.9	Energy absorbed by by cap-steel-beam structure during impact corresponding to different yielding strengths of beam steel	130

8.10	Time-histories of cap displacement corresponding to different yielding strengths of beam steel and maximum cap displacement vs. yielding strength of beam steel	130
8.11	Maximum bending moment diagrams of the structures during impact and deflections of the structures after impact corresponding to different yielding strengths of beam steel	131
8.12	Moment-curvature relationships of the I-cross-sections and moment-rotation relationships of single steel beams corresponding to different yielding strengths of beam steel	132
8.13	Impact force time-histories on the bridge pier for the whole impact process, for the first 0.10 s of impact process corresponding to different yielding strengths of beam steel and the maximum impact force vs. yielding strength of beam steel	132
8.14	Energy absorbed by by cap-steel-beam structure during impact corresponding to different beam unit numbers	133
8.15	Maximum bending moment diagrams of the structures during impact and deflections of the structures after impact corresponding to different beam unit numbers	134
8.16	Moment-curvature relationship of the I-cross-section and moment-rotation relationship of single steel beams corresponding to different beam unit numbers	135
8.17	Time-histories of cap displacement corresponding to different beam unit numbers and maximum cap displacement vs. beam unit number	135
8.18	Impact force time-histories on the bridge pier for the whole impact process, for the first 0.10 s of impact process corresponding to different beam unit numbers and the maximum impact force vs. beam unit number	136
8.19	Energy absorbed by cap-steel-beam structure during impact corresponding to different impact velocities	136
8.20	Time-histories of cap displacement corresponding to different impact velocities and maximum cap displacement vs. impact velocity	137
8.21	Moment-curvature relationship of the I-cross-section and moment-rotation relationship of single steel beams for different impact velocities	137
8.22	Maximum bending moment diagrams of the structure during impact and deflections of the structure after impact corresponding to different impact velocities	138
8.23	Impact force time-histories on the bridge pier for the whole impact process and for the first 0.10 s of impact process, respectively, corresponding to different impact velocities	139
8.24	Maximum impact force vs. impact velocity using the cap-steel-beam structure and without using the cap-steel-beam structure, respectively	140
8.25	The total number of beam units and the total mass of beam steel used by optimum cap-steel-beam structure vs. barge impact energy	143
8.26	Maximum cap displacement and maximum impact force on the bridge pier vs. barge impact energy using optimum cap-steel-beam structure	144
8.27	Maximum bending moment diagram of the structure during impact and deflection of the structure after impact corresponding to optimum cap-steel-beam structures for fully loaded barge of different impact velocities	145

8.28	Energy absorbed by optimum cap-steel-beam structure and the total impact energy during impact corresponding to impact scenarios IS_{31} , IS_{32} and IS_{33}	146
8.29	Proposed crashworthy devices of symmetrical configurations	147
9.1	RC pier column model considering soil-pile interactions and the layout of reinforcements	149
9.2	Simplified impact model for barge-pier impact analyses considering soil-pile interactions	150
9.3	Sensitivity of reliability index with respect to mean value of each random variable corresponding to two limit state functions	155

List of Tables

3.1	Geometric dimensions of Jumbo Hopper barge	18
3.2	Material parameters regarding barge steel	18
3.3	Material parameters regarding rigid pier column	19
3.4	Calibration of the present barge model against Yuan's barge model	20
3.5	Simulated rigid pier columns	21
3.6	Combinations of simulated impact velocities and impact angles using fully loaded barge and pier column $RP_F^{0.3}$	28
4.1	Coefficients of determination (R^2) corresponding to different values of α .	40
4.2	Coefficients of determination (R^2) corresponding to different values of θ for different values of α	42
5.1	Simulated linear elastic pier columns	45
5.2	Material parameters regarding linear elastic pier columns	45
5.3	Combinations of simulated barge masses and impact velocities for head-on impact corresponding to each linear elastic pier column	46
5.4	Combinations of simulated impact velocities and impact angles using fully loaded barge corresponding to each linear elastic pier column of square cross-section	65
6.1	Material parameters regarding RC beam members and drop hammer . . .	84
6.2	Parameters regarding RC pier column	87
6.3	Cross-section dimensions of flat RC pier columns	102
6.4	Cross-section dimensions of circular RC pier columns	103
6.5	Parameters regarding flat RC pier columns	103
6.6	Parameters regarding circular RC pier columns	103
7.1	Pre-specified parameters for parametric studies of pile-supported independent protective structures	114
8.1	Pre-specified parameters for parametric studies of cap-steel-beam structures	126
8.2	Relationships of I-cross-section dimensional parameters	140
8.3	Optimization model for optimizing cap-steel-beam structures	141
8.4	Impact scenarios considered for structure optimization	142
8.5	Pre-specified parameters for structure optimization	142
8.6	Optimum parameters, total masses of beam steel and configurations of optimum cap-steel-beam structures corresponding to different impact scenarios	143
8.7	Maximum cap displacements and maximum impact forces on the pier using or without using optimum cap-steel-beam structures corresponding to different impact scenarios	144
9.1	Statistical descriptions of random variables	152
9.2	Reliability indexes using two different reliability methods	153

List of Symbols

F_B	equivalent static barge impact force	9
u_b	barge bow crushing depth	9
W_b	barge impact energy	9
ρ_{vs}	mass density of barge steel	18
E_{vs}	Young's modulus of barge steel	18
ν_{vs}	Poisson's ratio of barge steel	18
f_y^{vs}	yielding strength of barge steel	18
ε_u^{vs}	failure strain of barge steel	18
m_b	barge mass	19
w_p	width of flat pier cross-section	19
l_p	length of flat pier cross-section	19
d_p	diameter of circular pier cross-section	19
σ_d	dynamic yielding stress	20
σ_s	static yielding stress	20
$\dot{\varepsilon}$	effective strain rate	20
F	impact force	20
F_{max}	maximum impact force	20
α	ratio of pier width/diameter to barge width	21
u_b^{max}	maximum barge bow crushing depth	22
θ	impact angle	28
u_1	yielding deformation of first non-linear spring in MSM	32
u_2	yielding deformation of second non-linear spring in MSM	32
F_{sy}	yielding force of first non-linear spring in MSM	32
F_{su}	ultimate force of first non-linear spring in MSM	32
F_{sp}	peak force of second non-linear spring in MSM	32
l_{bs}	length of two non-linear springs in MSM	32
v_p	prescribed constant velocity of complex barge model	36
R^2	coefficient of determination	37
h_i	height of barge impact position	43
h_p	height of pier column	43
m_s	superstructure mass	43
\mathbf{K}	stiffness matrix	43
\mathbf{P}	stiffness force	43
\mathbf{X}	displacement vector	44
\mathbf{X}_t	translational displacement vector	44
\mathbf{X}_r	rotational displacement vector	44
\mathbf{M}	mass matrix	44
D_{pt}	displacement at pier top	45
D_{pt}^{max}	maximum displacement at pier top	75
ρ_c	mass density of concrete	84
f_c	uniaxial compressive strength of concrete	84
D_{agg}	maximum aggregate size of concrete	84
ε_u^c	failure strain of concrete	84

d_{ls}	diameter of longitudinal reinforcement steel	84
ρ_{ls}	mass density of longitudinal reinforcement steel	84
E_{ls}	elastic modulus of longitudinal reinforcement steel	84
E_t^{ls}	tangent modulus of longitudinal reinforcement steel	84
f_y^{ls}	yielding strength of longitudinal reinforcement steel	84
ε_u^{ls}	failure strain of longitudinal reinforcement steel	84
d_{hs}	diameter of hoop steel	84
ρ_{hs}	mass density of hoop steel	84
E_{hs}	elastic modulus of hoop steel	84
E_t^{hs}	tangent modulus of hoop steel	84
f_y^{hs}	yielding strength of hoop steel	84
ε_u^{hs}	failure strain of hoop steel	84
ρ_h	mass density of drop hammer	84
E_h	elastic modulus of drop hammer	84
c	concrete cover depth	86
\mathbf{C}	damper matrix	88
\mathbf{q}	displacement vector of beam element	88
\mathbf{Q}	force vector of beam element	88
$\bar{\mathbf{q}}$	displacement vector of beam element without rigid body mode	88
$\bar{\mathbf{Q}}$	force vector of beam element without rigid body mode	88
\mathbf{T}	transformation matrix	89
$\mathbf{D}(x)$	section force vector	89
$\mathbf{b}(x)$	interpolation function	89
$\bar{\mathbf{K}}_E$	stiffness matrix of beam element without rigid body mode	89
$\mathbf{k}(x)$	section stiffness	89
\mathbf{K}_E	stiffness matrix of beam element with rigid body mode	89
ε_0	yielding strain of unconfined concrete	90
K	enhancement factor for confined concrete	90
ε_c	longitudinal strain of concrete	90
σ_c	longitudinal stress of concrete	90
ε_p	residual plastic strain of concrete	91
M	bending moment	92
M_{max}	maximum bending moment	93
m_c	mass of cap	109
d_{ct}	pile cross-section diameter	109
t_{ct}	thickness of pipe steel	109
h_{em}	pile embedded depth	109
h_{ct}	pile length	109
h_{sc}	scour depth	109
q	unit end bearing of pile	111
q_u	limiting unit end bearing of pile	111
Q_p	ultimate end bearing capacity of pile	111
f	unit shaft friction	111
δ	soil friction angle	111
f_u	limiting unit shaft friction	111
F_p	ultimate shaft friction	112
p_u	lateral bearing capacity of unit pile length	112
ϕ	soil internal friction angle	112
γ_s^{eff}	effective unit weight of soil	112

LIST OF SYMBOLS

P_p	ultimate lateral bearing capacity of soil	112
ε_{c0}	yielding strain of concrete confined by CFT	113
f_y^{ps}	yielding strength of pipe steel	114
E_c	elastic modulus of unconfined concrete	114
ρ_{ps}	mass density of pipe steel	114
E_{ps}	elastic modulus of pipe steel	114
E_t^{ps}	tangent modulus of pipe steel	114
ε_u^{ps}	failure strain of pipe steel	114
γ_s	unit weight of soil	114
W_{diss}^{barge}	energy absorbed by barge bow	115
W_{diss}^{pile}	energy absorbed by pile	115
W_{diss}^{soil}	energy absorbed by soil	115
N_{pl}	number of planes of beam units	125
f_y^{bs}	yielding strength of beam steel	125
N_{bu}	beam unit number in one plane	125
h_{bi}	depth of I-cross-section	125
w_{bi}	width of I-cross-section	125
t_{fi}	thickness of I-cross-section flanges	125
t_{wi}	thickness of I-cross-section web	125
ρ_{bs}	mass density of beam steel	126
E_{bs}	elastic modulus of beam steel	126
E_t^{bs}	tangent modulus of beam steel	126
ε_u^{bs}	failure strain of beam steel	126
W_{diss}^{csb}	energy absorbed by steel beams	126
D_{cap}	displacement of cap	126
D_{cap}^{max}	maximum cap displacement	126
γ	curvature of section	127
θ_b	relative rotation angle of two boundary sections of beam	127
F_{max}^{allow}	maximum allowable impact force on bridge pier	140
l_{sb}	length of steel beam	140
m_{sb}	total mass of steel beams	140
D_{max}^{allow}	maximum allowable displacement of cap	141
N_{bu}^{total}	total number of beam unit	141
f_m	p multi-plier	150
s_{sp}	center-to-center spacing of piles	151
$g(\mathbf{Z})$	approximated performance function	151
$G(\mathbf{Z})$	performance function	151
\mathbf{Z}	random variable vector	151
$\mu_{\mathbf{Z}}$	mean value of random variable	151
β	reliability index	152
M_y	bending moment about y axis	153
M_z	bending moment about z axis	153
AM_y	nominal moment capacity about y axis	153
AM_z	nominal moment capacity about z axis	153
F_y	shear force along y axis	153
F_z	shear force along z axis	153
AF_y	nominal shear capacity along y axis	153
AF_z	nominal shear capacity along z axis	153

List of Acronyms

FE	Finite-Element
RC	Reinforcement Concrete
CFRP	Carbon Fibre Reinforced Polymer
CVIA	Coupled Vessel Impact Analysis
UF	University of Florida
AVIL	Applied Vessel Impact Load
SDOF	Single-Degree-of-Freedom
MDOF	Multi-Degree-of-Freedom
MCM	Monte Carlo Method
RSM	Response Surface Method
FORM	First-Order Reliability Method
PC	Probability of Collapse
FBIM	Full Barge Impact Model
MSM	Mass-Spring Model
SIM	Simplified Impact Model
CMM	Coupled Multi-Degree-of-Freedom Model
JH	Jumbo Hopper
CFT	Concrete-Filled Steel Tube
LCS	Local Coordinate System
CMM	Coupled Multi-Degree-of-Freedom Model
SOPF	Second-Order Polynomial Function
TOPF	Third-Order Polynomial Function
FOPF	Fourth-Order Polynomial Function
LF	Logistic Function

Chapter 1

Introduction

1.1 Motivation for Research

A large number of bridges spanning over navigation waterways were built during the last decade. With the rapid growth of waterway transportation volume, the bridge piers located in navigation waterways are susceptible to vessel impact. As one of the extreme loading scenarios which have been widely investigated in recent years [1, 2, 3, 4, 5, 6, 7], barge impact loading can often lead to catastrophic consequences including human casualties and economic losses.

On 15 September 2001, four loaded barges crashed into the Queen Isabella Causeway in Texas, as shown in Fig. 1.1. As a result, a 240-foot (73.2 m) section of the causeway was knocked out and eight people lost their lives [8]. On 26 May 2002, two barges hit the I-40 highway bridge over the Arkansas River in Oklahoma, as shown in Fig. 1.2. A 580-foot (176.8 m) segment was sent into the river and fourteen people were killed when the vehicles plunged into the water [9]. On 15 June 2007, a cargo vessel fully loaded with sand crashed into one of the main pillars of Jiujiang Bridge located in Guangdong, China, as shown in Fig. 1.3. Approximately 200 meters of the bridge fell into the river, resulting in the loss of nine lives and great economic losses [10].

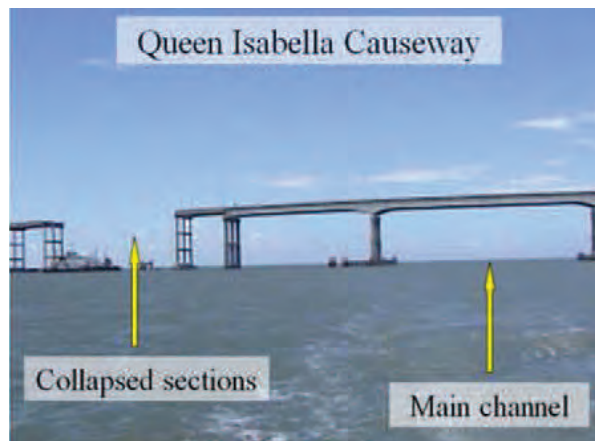


Figure 1.1: Collapse of Queen Isabella Causeway after being hit by four loaded barges on 15 September 2001 [11].

These are several examples of catastrophic vessel collision accidents which occurred in the past around the world. It was pointed out by Manen and Frandsen [12] and Larsen [13] previously that at least one major vessel-bridge collision accident of serious consequences occurred each year on average in the past. Barge collisions upon the bridge structures were also frequently reported.



Figure 1.2: Collapse of I-40 highway bridge after being hit by two barges on 26 May 2002 [11].



Figure 1.3: Collapse of Jiujiang Bridge after being hit by the cargo vessel on 15 June 2007 [11].

These catastrophic vessel collision accidents have led to substantial scientific investigations on vessel-bridge impact analyses. However, the focus of many previous studies is on ship impact analyses. As barges and ships share fundamental differences in shapes and inner structures, the corresponding studies pertaining to ship impact analyses cannot be directly applied to barge impact analyses [14]. Empirical formulas based on equivalent static method such as those provided by AASHTO Guide Specification [15] are widely used in bridge designs against barge impact. However, barge impact is a highly dynamic process. The equivalent static analyses ignore important dynamic effects, i.e. inertial forces and damping forces, involved in the impact event. In order to take such dynamic effects into account, substantial studies on barge impact analyses were conducted in literature using experimental impact tests [16, 17, 18, 19, 20] or finite-element simulations [4, 5, 6, 21, 22, 23, 24, 25, 26, 27, 28]. However, the dynamic barge impact analyses using experimental impact tests or finite-element simulations often require substantial investment of time and effort. In addition, conducting experimental impact tests can be rather costly.

As an alternative strategy, simplified impact models are currently extensively used for barge-pier impact analyses [29, 30, 31]. However, factors such as strain rate, material

properties of impacted structures, etc, are often not fully considered by these existing simplified models, thus their applications to engineering designs are often quite limited. Several problems regarding model simplicity or prediction accuracy often exist in these existing models [7, 14]. In addition, these simplified models are often only tested for a limited number of impact scenarios. Many factors such as barge mass, impact velocity, impact angle, material properties of barge structural components, strain rate, pier shape, pier size, material properties of pier members, soil-pile interactions, etc, are influential upon the barge impact process. However, a thorough assessment of the simplified models including all these factors can rarely be found in literature.

Several questions remain to be answered - How to predict the time-histories of barge impact force efficiently with sufficient accuracy for a wide range of impact scenarios? How to predict the dynamic responses of bridge piers subjected to barge impact efficiently with sufficient accuracy for a wide range of impact scenarios? How to protect the bridge pier from barge impact loads? These questions form the motivations for the studies in this dissertation.

1.2 Objective of Research

The main objective of this dissertation is to develop simplified models which can replicate the complex full barge impact models with sufficient accuracy for a wide range of impact scenarios. Using such simplified models to devise new crashworthy devices for pier protection from barge impact and to conduct reliability analyses of bridge piers subjected to barge impact serves as another objective of this dissertation.

1.3 Contribution of Research

The contribution of this research is summarized as follows:

- A thorough literature review is conducted on vessel impact analyses. The relevant work in literature pertaining to this topic is discussed in detail.
- A simplified non-linear mass-spring model (MSM) is developed to replicate the complex barge model. An optimization model is proposed to generate the model parameters introduced in MSM.
- A group of regression formulas is developed to calculate the MSM parameters. The quality of these regression formulas is well assessed using correlative studies.
- The coupled multi-degree-of-freedom (MDOF) model is developed by coupling MSM with the pier column at the impact position to predict the impact force time-history and dynamic pier responses for a given impact scenario. The prediction quality of the coupled MDOF model (CMM) is thoroughly assessed for a wide range of impact scenarios using linear elastic pier columns.
- Material non-linearity of pier column members is considered by CMM using fibre beam elements. Parametric studies are conducted using RC pier columns of different configurations to assess the prediction quality of CMM involving material non-linearity of pier column members.
- The simplified impact model considering soil-pile interactions and geometric non-linearity is developed based on CMM. Using the simplified model, the

energy-dissipation capacity of pile-supported independent protective structures is evaluated considering several design parameters.

- A new type of crashworthy device comprised of a supported or floated cap connected to the bridge pier using a series of steel beams of I-cross-section is devised and its effectiveness is investigated using the proposed simplified impact model developed based on CMM. A mathematical optimization model is developed accordingly to achieve cost-optimum design of the proposed crashworthy device for a given impact scenario with constraints generated by the prescribed design requirements.
- The simplified impact model considering soil-pile interactions and pile-group effects is developed based on CMM for dynamic analyses of RC pier column subjected to barge impact. Using the proposed model, reliability analyses of RC pier column subjected to barge impact are conducted with existing reliability methods and sensitive random variables are figured out by sensitivity analyses.

1.4 Organization of Dissertation

The dissertation is organized as follows:

Chapter 2 conducts a thorough literature review of vessel impact analyses. The existing experimental impact tests and analytical models pertaining to this topic are summarized. A state of the art overview of the design of protective structures against vessel impact and reliability analyses of bridge piers subjected to vessel impact are also presented.

Chapter 3 develops the complex finite-element barge model which is used for the studies in this dissertation. The descriptions of the complex barge model, i.e. material models, element types, contact definition, etc, and the calibration of the complex barge model against one literature barge model are included in this chapter. The full barge impact model (FBIM) using the proposed complex barge model and rigid pier column is developed to study the influences of pier shape, pier size, impact velocity and impact angle upon barge bow crushing behavior.

Chapter 4 introduces a simplified non-linear MSM which is developed to replicate the complex barge model. The optimization model for determining the model parameters introduced in MSM is proposed. The regression formulas in terms of pier shape, pier size, impact velocity and impact angle are developed for calculating the model parameters.

Chapter 5 develops the CMM to efficiently predict the impact force time-history and dynamic pier responses for a given impact scenario. The prediction quality of CMM is thoroughly assessed in this chapter for a wide range of impact scenarios using linear elastic pier columns of several different shapes and sizes.

Chapter 6 introduces material non-linearity of pier column members to CMM using fibre beam elements. The concrete model used in the RC pier column model is validated by a series of drop hammer impact tests on RC beams. The FBIM using the validated RC pier column model is then used as the benchmark model to assess the prediction quality of CMM involving material non-linearity of pier column members.

Chapter 7 develops the simplified impact model based on CMM considering soil-pile interactions and geometric non-linearity. Using this simplified model, parametric studies

are conducted to evaluate the energy-dissipation capacity of pile-supported independent protective structures considering several design parameters.

Chapter 8 devises a new type of crashworthy device using a series of steel beams for pier protection from barge impact and its effectiveness is investigated using the simplified model developed based on CMM considering geometric non-linearity. A mathematical optimization model is developed accordingly to achieve cost-optimum design of the proposed crashworthy device for a given impact scenario with constraints generated by the prescribed design requirements.

Chapter 9 develops the simplified impact model considering soil-pile interactions and pile-group effects based on CMM for dynamic analyses of RC pier column subjected to barge impact. Reliability analyses are conducted for the RC pier column subjected to barge impact using the simplified model with existing reliability methods. Sensitivity analyses are conducted using Response Surface Method to figure out the sensitive random variables.

Chapter 10 provides conclusions derived from the studies in this dissertation and recommendations for future studies are offered.

Chapter 2

Literature Review

2.1 Introduction

In this chapter, important historical research pertaining to vessel impact analyses are discussed in detail and the importance of simplified impact models is highlighted. A state of the art overview of the design of protective structures against vessel impact and reliability analyses of bridge piers subjected to vessel impact is also presented.

2.2 Strategies for Vessel Impact Analyses

Experimental impact tests and analytical models are two commonly-used strategies in literature to conduct vessel-pier impact analyses. Empirical formulas, finite-element simulations and simplified impact models are currently extensively used for bridge designs against vessel impact. These strategies are summarized as shown in Fig. 2.1.

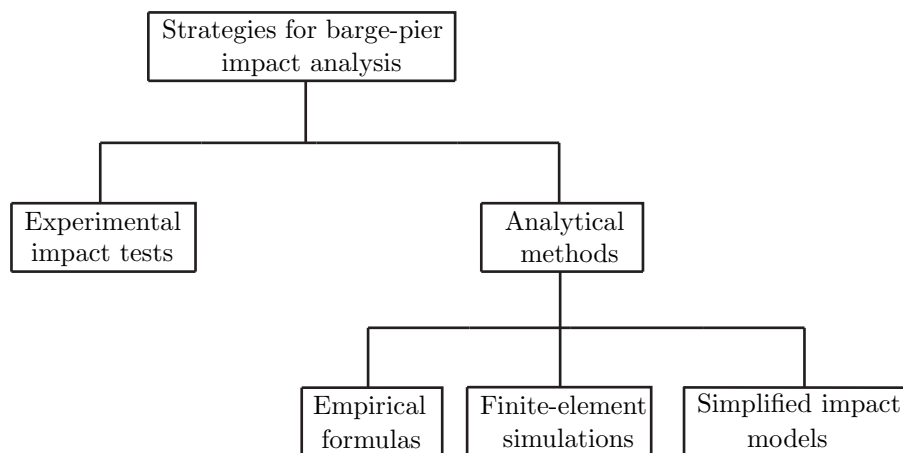


Figure 2.1: Strategies for vessel-pier impact analyses.

2.2.1 Experimental Impact Tests

Although a large number of vessel impact accidents occurred in the past, the number of experimental impact tests which were conducted in literature is very limited. The vessel impact can be classified into two categories based on the vessel type, i.e. ship impact and barge impact. The earliest ship impact tests were conducted by Minorsky in 1959 [32]. The research focused on studying the remaining vessel damage after impact. An empirical formula was proposed to describe the relationship between the deformed steel volume and the absorbed impact energy based on the data obtained from the twenty-six impact tests. Woisin conducted a total of twenty-four impact tests using scaled ship models (1:7.5 to 1:12) from 1967-1976 [33] for the sake of protecting nuclear-powered

ships from collision against other ships. An empirical formula was developed accordingly to quantify the equivalent impact force based on the ship size and impact velocity.

However, ship vessel and barge vessel share fundamental differences in bow shapes and inner structures, thus the bow crushing behavior of barge vessel cannot be readily extrapolated from ship impact tests. Meir-Dornberg once conducted dynamic loading with a drop hammer and static loading on barge models of reduced-scale (1:4.5 to 1:6) in 1983 to quantify the barge impact loading during impact [16]. Based on the data obtained from the impact tests, the empirical formulas were developed relating the impact energy, barge bow crushing depth and barge impact force. It was concluded from the impact tests that the barge bow force-deformation relationship is not strongly related to the loading type, i.e. dynamic loading or static loading, as shown in Fig. 2.2, where u_b is the barge bow crushing depth, F_B is the impact force and W_H is the hammer impact energy.

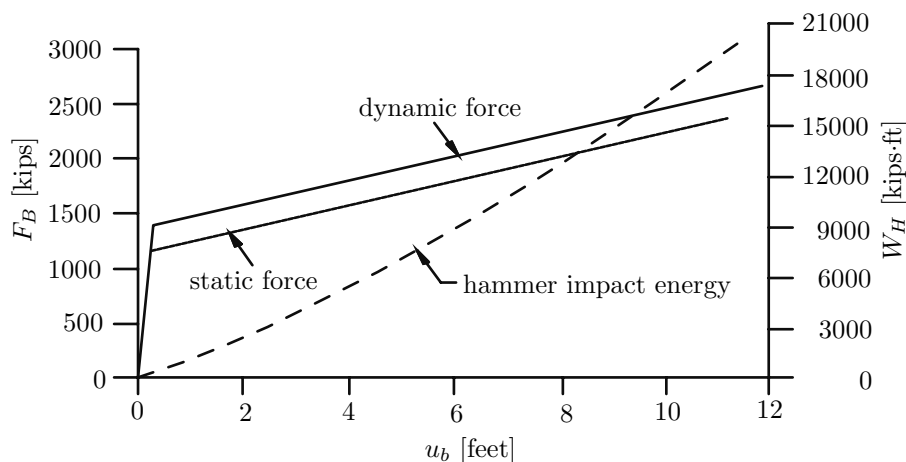


Figure 2.2: Relationship of hammer impact energy, barge bow crushing depth and impact force based on the impact tests conducted by Meir-Dornberg [15].

Using impact data from scaled impact tests could introduce uncertainty errors when applied to describe the full-scale impact event, especially when they cannot be fully validated using data from full-scale impact tests. As the drop hammer is not representative of a real bridge pier, Meir-Dornberg's impact tests failed to reflect the dynamic interactions between the barge and the bridge pier during impact. These problems necessitate the conduction of impact tests using full-scale barge model. The US Army Corps of Engineers once conducted a series of impact tests using full-scale barge flotilla impacting against the lock gates [17] and the lock wall [18, 19]. Sensors were employed to record the force, velocity and acceleration time-histories of the impacting barge, the structural responses of the lock wall at the impact position and barge-to-barge lashing forces during impact. However, there exist fundamental structural differences between the bridge piers and the lock gates or lock walls, thus the data obtained from the impact tests cannot be readily applied to bridge designs against barge impact.

In 2004, University of Florida (UF) conducted a full-scale experiment of barge impact on the old St. George Island Causeway Bridge [20, 34, 35]. This is the first full-scale test of barge impact on bridge piers which serves as a benchmark for illustrating the physical phenomena involved in real barge-pier impact events. Two bridge piers, i.e. Pier-1 and Pier-3 as shown in Fig. 2.3, were selected for conducting the impact tests. Sensors including accelerometers, stain gages and load cells were positioned at different

locations on the barge, the piers, the piles and the superstructure to record the impact force time-history and dynamic pier responses. Fig. 2.4 shows the barge impact tests on Pier-1 and Pier-3, respectively.

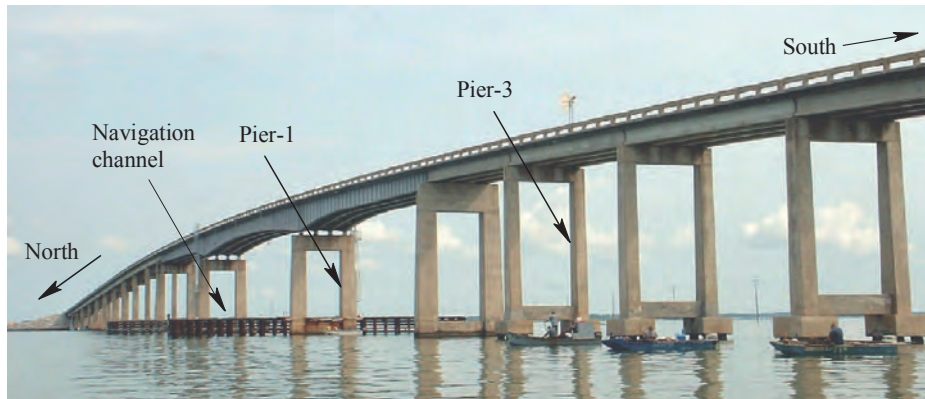


Figure 2.3: Bridge piers selected for conducting the barge impact tests [20].

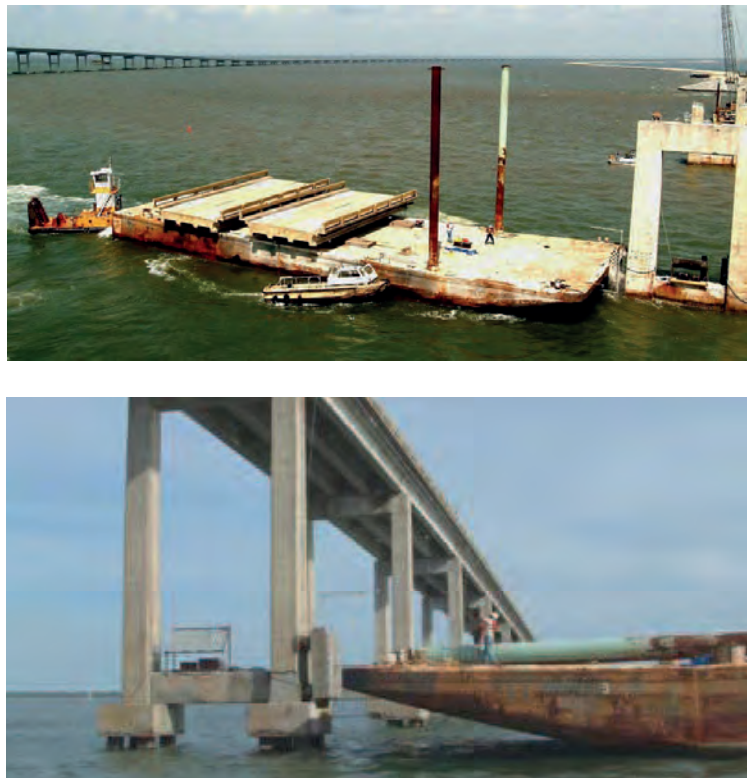


Figure 2.4: Barge impact tests on Pier-1 (top) and Pier-3 (bottom) of the old St. George Island Causeway Bridge [36].

In total fifteen impact tests were conducted on the two piers with different barge impact energy and pier superstructure conditions. The test results indicate that the maximum experimentally measured dynamic impact loads follow a linear trend line up to a transition point after which the impact loads plateau with respect to further increases in kinetic impact energy [20]. However, the experimental plateau level of the impact loads is lower than that predicted by AASHTO Guide Specification. Impact tests upon Pier-3 which is of small flexibility using small barge weight and low impact velocity were also conducted, and the corresponding results indicate that the maximum dynamic

impact loads are typically higher than the equivalent impact force predicted by AASHTO Guide Specification.

Experimental impact tests can provide convincing benchmarks for dynamic analyses of vessel impact events. However, conducting such experiments is both costly and time-consuming. It is often difficult to achieve the expected impact scenarios due to factors such as unpredictable weather conditions, water flow, etc. The number of experimental impact tests in literature is thus quite limited. The great operation difficulties as well as high expenses and substantial investment of time and energy involved in the experimental impact tests render them unpractical for many scientific studies. The analytical methods using empirical formulas, finite-element simulations or simplified impact models are thus extensively used.

2.2.2 Empirical Formulas

Different empirical formulas were developed in literature for calculating barge impact forces. The formulas provided by codes such as AASHTO Guide Specification [15] and Eurocode [37] are most extensively used.

2.2.2.1 The AASHTO Guide Specification

The empirical formulas adopted by AASHTO Guide Specification were developed based on the data obtained from the research conducted by Meir-Dornberg in Germany in 1983. Meir-Dornberg conducted the hammer impact tests using scaled barge models to study the deformation force of the barge bow. Empirical formulas based on the experimental results were developed as follows [16]:

$$F_B = \begin{cases} 60.0u_b, & u_b < 0.1\text{m} \\ 6.0 + 1.6u_b, & u_b \geq 0.1\text{m} \end{cases} \quad (2.1)$$

where F_B is the equivalent static barge impact force [MN], u_b is the barge bow crushing depth [m] calculated by:

$$u_b = (\sqrt{1.0 + 0.13W_b} - 1) \cdot 3.1 \quad (2.2)$$

where W_b is the barge impact energy [MNm].

The AASHTO Guide Specification adopted the above empirical formulas by introducing two modification coefficients as follows:

$$F_B = \begin{cases} 60.0u_bR_B, & u_b < 0.1\text{m} \\ (6.0 + 1.6u_b)R_B, & u_b \geq 0.1\text{m} \end{cases} \quad (2.3)$$

$$u_b = (\sqrt{1.0 + 0.13W_b} - 1) \cdot \left(\frac{3.1}{R_B}\right) \quad (2.4)$$

where R_B is equal to the ratio of barge width [m] to 10.6 m.

The formulas adopted by AASHTO Guide Specification are based on impact tests conducted by Meir-Dornberg using scaled barge models, and may not accurately predict the full-scale barge impact loading on bridge piers. Several previous studies have indicated that the shape and size of pier column as well as impact angle are very influential upon the impact force and barge bow crushing behavior [21, 22, 38]. However, these effects are not included in the empirical formulas. The rigid hammer used in

Meir-Dornberg's experimental tests is not analogous to real bridge pier which also absorbs impact energy during impact. The empirical formulas indicate that the impact force increases monotonically with respect to barge bow crushing depth, whilst several previous studies have indicated that the barge bow generally undergoes a plastic-yielding session during impact [21, 22, 39]. The important dynamic effects such as inertia forces and damping forces involved in the barge impact events are totally ignored by the empirical formulas.

2.2.2.2 The Eurocode

The Eurocode proposed the formulas for calculating the dynamic impact force based on the deformation energy of the vessel. For vessels traveling in inland waterways the formulas are as follows [37]:

$$F_{dyn} = \begin{cases} 10.95 \cdot \sqrt{W_{def}}, & W_{def} \leq 0.21\text{MNm} \\ 5.0 \cdot \sqrt{1.0 + 0.128 \cdot W_{def}}, & W_{def} > 0.21\text{MNm} \end{cases} \quad (2.5)$$

where F_{dyn} is the dynamic design impact force [MN]; W_{def} is the vessel deformation energy in MNm which is equal to the total kinetic energy of the vessel W_b for a head-on impact and is calculated by the following equation for a lateral impact with angle $\psi < 45.0^\circ$:

$$W_{def} = W_b(1 - \cos\psi) \quad (2.6)$$

If a dynamic structural analysis is required, the impact force is modeled as a half-sine-wave pulse for $F_{dyn} < 5.0$ MN (elastic impact) and a trapezoidal pulse for $F_{dyn} > 5.0$ MN (plastic impact), as shown in Fig. 2.5. The loading duration and other details are also presented in Fig. 2.5. In Fig. 2.5, t_r is the elastic elapsing time [s], t_p is the plastic impact time [s], t_e is the elastic response time [s], t_a is the equivalent impact time [s], t_s is the total impact time [s] which is equal to the summation of t_r , t_p and t_e for plastic impact, F_0 is the elastic-plastic limit force (5.0 MN). The values of t_a , t_r , t_p , t_e and F_D are calculated by the following equations [37]:

$$t_a = 2.0 \cdot \sqrt{m^*/c_v} \quad (2.7)$$

$$t_r = \begin{cases} \sqrt{m^*/c_v}, & F_{dyn} \leq 5.0\text{MN} \\ x_e/v_n, & F_{dyn} > 5.0\text{MN} \end{cases} \quad (2.8)$$

$$t_p = m^* \cdot v_n/F_D \quad (2.9)$$

$$t_e = \pi/2 \cdot \sqrt{m^*/c_v} \quad (2.10)$$

$$F_D = (F_0 + F_{dyn})/2.0 \quad (2.11)$$

where c_v is the elastic stiffness of the vessel (60.0 MN/m); x_e is the elastic deformation (0.1 m); v_n is equal to the vessel sailing speed (v_r) for head-on impacts and $v_r \cdot \sin\psi$ for

lateral impacts with angle ψ ; m^* [10^6kg] is equal to the total mass of vessel for head-on impacts and (m_1+m_{hyd}) for lateral impacts where m_1 is the mass of the directly colliding vessel (10^6kg) and m_{hyd} is the hydraulic added mass [10^6kg].

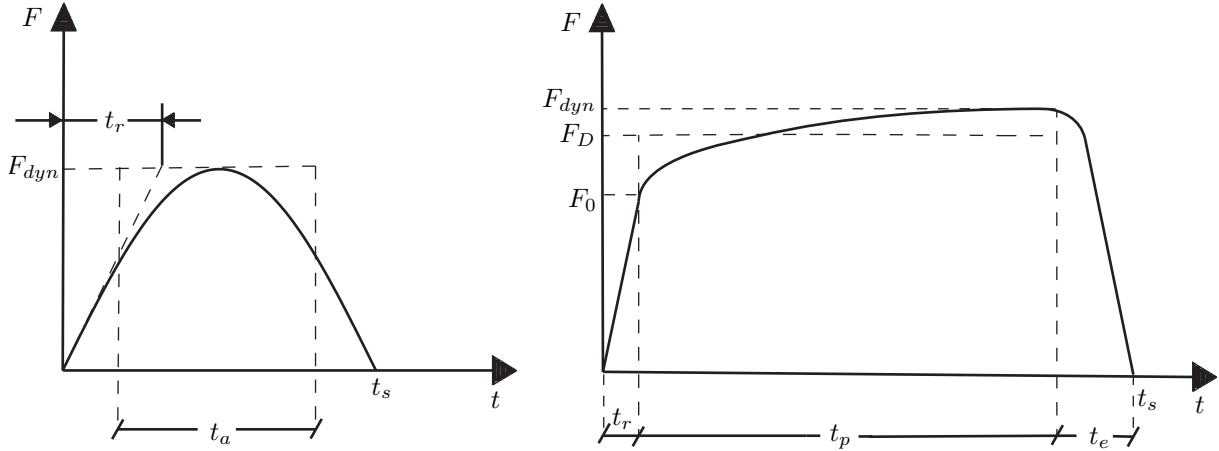


Figure 2.5: Impact force time-history determined by Eurocode for vessels traveling in inland waterways [37],
 (left) elastic impact,
 (right) plastic impact.

The Eurocode provides a simple approach for deciding the impact force time-history considering the influences of barge impact energy and impact angle. However, similar to the AASHTO empirical formulas, the Eurocode formulas ignore the influences of pier shape and pier size upon the impact force. Several previous studies [4, 14] have indicated that the stiffness and material properties of pier column have significant influences upon the impact force. However, these factors cannot be considered by the Eurocode formulas.

2.2.3 Finite-Element Simulations

The FE simulations require numerical modeling of the vessel and the bridge pier using an assembly of elements. The numerical solutions of such an FE model can be obtained by commercial software such as LS-DYNA. The impact force time-history and dynamic pier responses can be obtained accordingly. The FE simulations have been extensively used by many research institutions around the world.

Consolazio et al. [21] used FE simulations to study the static crushing behavior of the barge using multiple pier-shaped impactors, and it was found that the shape and size of the impactor influence the barge bow force-deformation relationship and that the impact force does not necessarily increase monotonically with the increase of crushing depth. Yuan [22, 23] developed the complex FE barge model which was employed for conducting a series of single-barge simulations and multi-barge-flotilla simulations. The influences of impact velocity, pier stiffness, pier shape and pier size upon the impact force time-history and barge bow crushing behavior were thoroughly studied. It was concluded from Yuan's studies that the impact forces are limited to the plastic load-carrying capacity of the barge bow; the increase of pier width can result in the increase of impact force, but the size influence of square pier column is more apparent than that of circular pier column; the maximum impact forces are very sensitive to the stiffness variation of weaker piers. Sha and Hao [4, 5] developed the FE barge impact model in which the material non-linearity of the pier column members were included

after calibrations using the pendulum impact tests on a scaled circular RC column. The influence of material non-linearity of the pier column members was then studied using the numerical model and it was concluded that the non-linear bridge pier response and damage in the impact process significantly affect the barge-pier impact response and should not be neglected. Sha and Hao [6] also conducted the numerical simulations of full-scale barge impact on the carbon fibre reinforced polymer (CFRP) strengthened pier column. It was found that the CFRP strengthening technique cannot reduce the maximum impact force but can mitigate the damage of the pier during impact.

Compared with experimental impact tests, FE simulations can save time and cost and can even be employed to simulate the impact scenarios that are non-testable. However, FE simulations still suffer from several fundamental problems. Generally, a substantial investment of time and effort is required for non-linear modeling of the vessel, the piles, the connecting beams, and the soil. In addition, the computational demands involved in conducting high-resolution non-linear contact/impact analyses often demand super-computing resources and excessive computing time [29, 40]. For these reasons, simplified models that can predict impact force time-history and dynamic pier responses with sufficient accuracy are often required by engineering designs and scientific studies.

2.2.4 Simplified Impact Models

Several simplified impact models, i.e. the Coupled Vessel Impact Analysis (CVIA) technique introduced by UF [29], the simplified impact model proposed by Yuan [30], etc, were developed in literature for predicting the dynamic bridge-pier impact process.

The CVIA technique is implemented by coupling the barge mass with the pier structure using a non-linear spring representing the barge bow crushing behavior, as shown in Fig. 2.6. The crushing curves of barge bow corresponding to different pier shapes, pier sizes and impact angles were studied using quasi-static crushing analyses and a simple procedure was developed to obtain the force-deformation relationship of the non-linear spring [38, 41]. The CVIA technique has been validated using both experimental data and FE simulation results [42, 43]. This technique has been widely used in recent studies [44, 45]. The barge bow crushing model was also employed by Luperi and Pinto [46]. As an alternative to the CVIA technique, the Applied Vessel Impact Load (AVIL) technique was developed to generate the impact force time-history based on a barge bow force-deformation relationship of interest [36]. Yet another alternative, which consists of a frequency-based approach to predict the maximum pier response, and makes use of impact response spectra, was proposed in Ref. [47]. Material non-linearity of the pier column members can be considered by the proposed strategies.

Yuan featured the barge mass as a lumped mass and the barge bow as a group of elastoplastic-collapse elements that become active or inactive in a sequential order, as shown in Fig. 2.7. The model allows a physical interpretation of the force-deformation relationship of barge bow [30]. Yuan's simplified model introduced a group of model parameters, the values of which can be obtained by the proposed optimization models. The bridge pier was modeled by a cantilever using two concentrated masses representing the superstructure mass and the mass at the impact position, respectively. The superstructure constraints were modeled by translational springs and rotational springs. The response spectrum analyses were conducted to estimate the maximum displacements at the impact position and the pier top for a given rectangular pulse force. Such response spectrum analyses have also been used by previous research regarding vessel-bridge